Non-destructive lab-scale monitoring of carbonation propagation in cementitious systems using the measurement of intrinsic electrical property

Materials and Structures (2025) 58:55
https://doi.org/10.1617/s11527-025-02576-2

ORIGINAL ARTICLE

Non-destructive lab-scale monitoring of carbonation propagation in cementitious systems using the measurement of intrinsic electrical property

Arezou Babaahmadi · Luping Tang · Liming Huang · Sahar Iftikhar · Ingemar Löfgren

Received: 28 May 2024 / Accepted: 10 January 2025

Abstract Monitoring carbonation in concrete is crucial for assessing the long-term durability of structures, particularly as sustainability efforts increasingly incorporate supplementary cementitious materials (SCMs) to reduce clinker content. While beneficial, SCMs alter the pore structure and pore solution chemistry, necessitating advanced methods to evaluate carbonation progression. Traditional techniques, such as splitting specimens and using pH indicators like phenolphthalein to detect changes in alkalinity, are destructive and primarily designed for ordinary Portland cement (OPC), limiting their effectiveness for SCM-incorporated systems. This paper presents the development of a novel lab-scale carbonation monitoring method based on conductivity measurements in the cementitious matrix. The proposed method examines how carbonation impacts the electrical conductivity of concrete, enabling in-situ monitoring of carbonation propagation in mortar specimens using mini-sensors embedded within the material. These mini-sensors consist of 10 sets of stainless steel 4-point Winner electrodes, spaced 2.54 mm apart, ensuring accurate conductivity measurements. By strategically placing these mini-sensors within the cementitious matrix, real-time measurements can be carried out, allowing for continuous monitoring of carbonation progression. The method provides new insights into how carbonation impacts the electrical properties of concrete, revealing dynamic changes such as a distinct peaking behavior in conductivity at the reactive carbonation front. This feature enables identification of partial carbonation front, which traditional colorimetric methods cannot detect. The results validate the method's effectiveness for OPC system and indicate its applicability when SCMs are incorporated.

Keywords Carbonation · Electrical conductivity · Methodological development · Test method

1 Introduction

Cementitious construction materials have enormous importance for the sustainable development of the built environment due to their availability, excellent performance, and long service life. However, due to the large volumes used, cement production is associated with high environmental footprints, which is a complex and multidimensional challenge to address.

Application of supplementary cementitious materials (SCMs), producing so called composite binders, represents one of the most viable solutions to reduce negative environmental impact of cements

A. Babaahmadi (✉) · L. Tang · L. Huang · S. Iftikhar · I. Löfgren
Department of Architecture and Civil Engineering, Chalmers University of Technology, Gothenburg, Sweden
e-mail: arezou.ahmadi@chalmers.se

I. Löfgren
Thomas Concrete Group AB – C-lab, Gothenburg, Sweden

Published online: 03 February 2025

[1]. However, reducing clinker content raises concerns about potential neutralization of the concrete pore solution, meaning a decrease in pH levels. This reduction in pH may subsequently increase the risk of reinforcement corrosion due to carbonation [2]. It is important to note that aside from the very importance of reinforcement corrosion, carbonation can also affect the hydrate phase assemblage, solid volumes, and pore structure, i.e. the physio-chemical properties. Depending on the cementitious binder's chemistry these changes can be accounted for as positive or negative in terms of durability and engineering properties of the concrete produced with composite binders. The positive changes are observed when a finer pore structure is obtained due to increased solid volumes, hence, diffusivity of CO_2 is reduced in the system. As it is noted in [2], in systems where SCMs significantly reduce the portlandite content, carbonation can be accelerated within the primary CO_2-binding phases (C–S–H and C–A–S–H). This carbonation process significantly contributes to carbonation shrinkage, especially notable in C(-A)–S–H phases with low calcium-to-silicon ratios, leading to pore structure coarsening and decreased mechanical strength. These effects are pivotal to consider in the assessment of concrete with SCMs, as carbonation not only lowers the overall pH but also induces pore structure coarsening, thereby compromising the material's resilience against chemical or physical degradation.

Therefore, further understanding of relationships between carbonation propagation and microstructural changes (such as probably generation of microcracks) alongside the changes in the pore solution chemistry and the effect of these parameters on engineering properties of the material, such as mechanical strength, is critical for proper evaluation of the new generation of composite binders. In line with this aim, a non-destructive method to monitor propagation of carbonation front is a necessity. In current practice, the carbonation depth is measured by spraying a colour indicator solution on a freshly broken cementitious surface. Although the method has accuracy and is represented in the harmonized standard for measurement of carbonation front (EN 13295:2004) [3], being destructive, it lacks the possibility of utilizing the same specimen in parallelly coupled investigations. In addition, non-destructive methods may have a higher precision as no visual judgment is required as in colorimetric methods. As reported in [4], visual observation of colour change boundaries results in the need for human judgement to be applied; therefore for comparison studies such as the round robin test presented in this review article, each involved laboratory applied its established processes and expertise in defining exactly how faint the colour indicator colouration would be at the point defined as the carbonated-uncarbonated boundary. Moreover, a non-destructive method facilitates smaller number of specimens required through the course of investigations and can be further up-scaled for in-situ monitoring of concrete properties in service.

Electrical resistivity, with its flexibility, effectiveness, and non-destructive nature, is poised to be utilized for continuous measurements. Commonly employed in geophysics, methods for measuring electrical properties aid in exploring and characterizing the underlying structures of the earth's surface, providing valuable insights into the terrain and lithological composition of the subsurface [5–8]. The electrical properties of cementitious systems, specifically those measured under alternating current (AC) conditions, have been widely studied in the literature to analyse the properties of cementitious matrices [9–15]. Determination of electrical resistivity is also a standardized method for investigating properties of hardened concrete (EN-12390–19) [16]. The application of this technique as a qualitative way for better understanding of the hydration evolution in cementitious matrices [17, 18] as well monitoring durability of concrete [19–21], is discussed in the literature. However, up to the knowledge of the authors no record of using this technique to monitor carbonation profiles in cementitious specimens is reported in the literature.

Electrical resistivity refers to a system's ability to hinder the flow of electrical current, while conductivity represents its reciprocal. As is well-documented, carbonation influences phase compositions, which in turn affects the chemistry of the pore solution and the microstructure.[2]. These changes can be reflected through conductivity measurements [9–15].

In this paper, a non-destructive monitoring of carbonation propagation in cementitious systems using the measurement of intrinsic electrical property is presented. The credibility of the method to reflect the propagation of carbonated front is confirmed by the colorimetric method, spraying a colour pH-indicator

solution on a freshly broken cementitious surface of the samples. The method enables in-situ monitoring of carbonation propagation in standard mortar specimens through application of embedded mini-sensors for measurement of electrical properties. By strategically embedding these mini-sensors within the cementitious matrix, real-time measurements can be conducted, enabling continuous monitoring of carbonation progression. This approach offers advantages in terms of cost-effectiveness, simplicity, and non-destructiveness compared to traditional destructive laborious methods.

The primary focus of this paper is the methodological development of a non-destructive laboratory scale carbonation monitoring technique, initially validated on Portland cement (OPC)-based systems. To further illustrate the method's applicability for cementitious system with incorporation of SCMs, additional measurements have been included for a ternary slag-limestone incorporated system. It should however be noted that the credibility of electrical property measurements in binders with incorporation of SCMs is well-supported in the literature [17, 21–23].

2 Materials and methods

2.1 Non-destructive monitoring system

The non-destructive monitoring system developed in this study is visualized in Fig. 1. The system is composed of an in-house fabricated carbonation chamber equipped with an in-situ monitoring of changes in conductivity of cementitious systems while undergoing carbonation. The carbonation chamber is equipped with sensors detecting concentration of CO_2 as well as temperature and relative humidity in the chamber. The desired relative humidity is achieved by

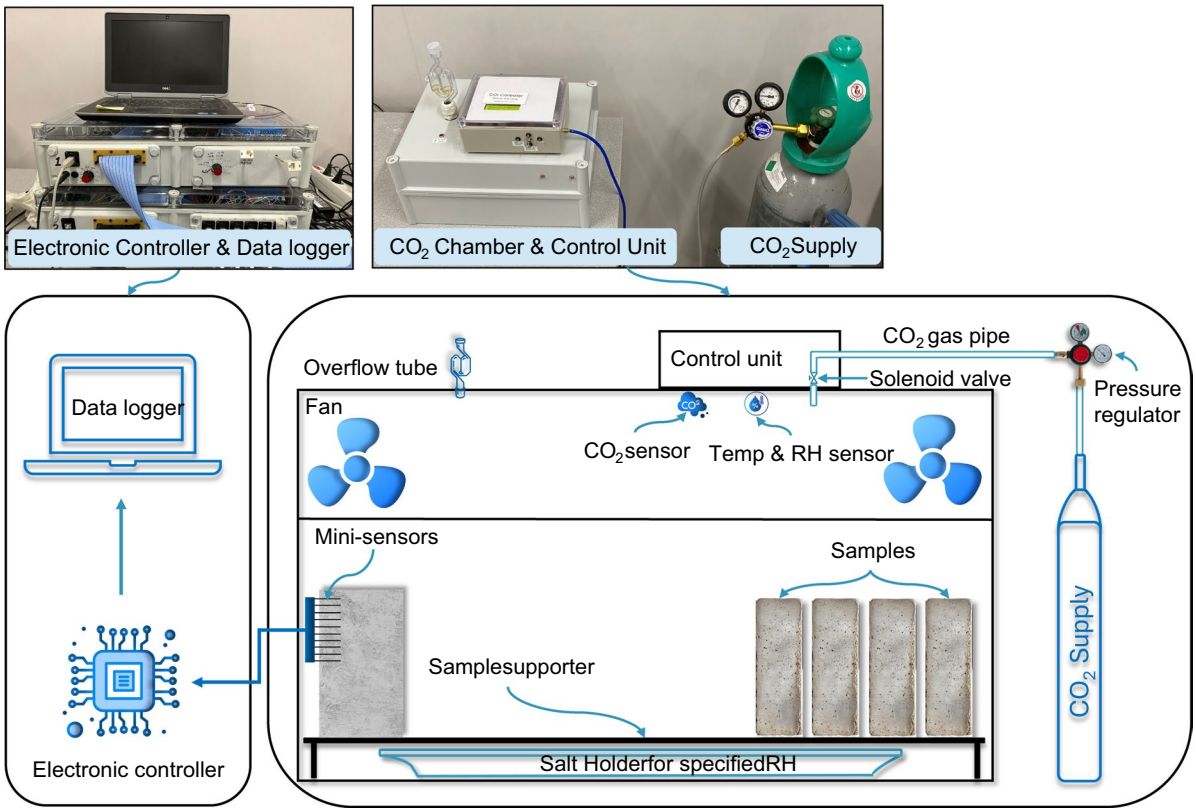

Fig. 1 Non-destructive monitoring system for in-situ measurement of conductivity in mortar specimens undergoing accelerated carbonation

employing various saturated salt solutions to generate the specific humidity level needed.

The electrical conductivity of concrete is measured by a four-electrodes method to minimize the effect of polarization. The electronic controller and the data acquisition system have been developed by authors [21, 24] intended for monitoring hydration and strength development of low CO_2 concrete. To accommodate the measurements for mortar prisms, mini-sensor consisting of 10 sets of 4-points-Winner electrodes (stainless steel needles) for conductivity measurements were cast embedded in mortar specimens. The 4-point resistivity measurement method involves placing four electrodes along the surface of the specimen, with an outer pair used to apply a constant current and an inner pair to measure the resulting voltage. This setup minimizes the influence of electrode polarization and contact resistance, providing an accurate measurement of the sample's intrinsic electrical properties. The distance between 4-points-Winner electrodes is 7.62 mm (0.3'') suitable for a maximum size of aggregate of 2–4 mm, whilst the distance between two sets is 2.54 mm (0.1''). As a result, detection of changes in the electrical conductivity of cementitious matrices is achieved at a depth interval of 2.54 mm (0.1''), and up to about 23–25 mm from the surface depending on the position of the first set of electrodes. The arrangement of the mini-sensors is illustrated in Fig. 2, provides a comprehensive overview of sensor configuration. Fig. 2a illustrates a sample with embedded sensors, where unidirectional carbonation occurs from top to bottom as indicated by the arrow. Fig. 2b presents the blueprint of the sensor grid layout in cross-section, while Fig. 2c displays the cross-section of the mortar prism with the embedded sensor arrays.

2.2 Cementitious matrices

The cementitious materials in this study are mortars prepared according to SS-EN 196–1. The materials used includes an ordinary Portland cement CEM I 52.5 R with a Blaine surface of 525 m2/kg Bremen with a Blaine surface of 420 m2/kg as well as limestone from Nordkalk with a D50 = 18 µm. The chemical composition of the binders is presented in Table 1. Motar mixture was prepared with slag and limestone substitutions. In the ternary blend, 35% of

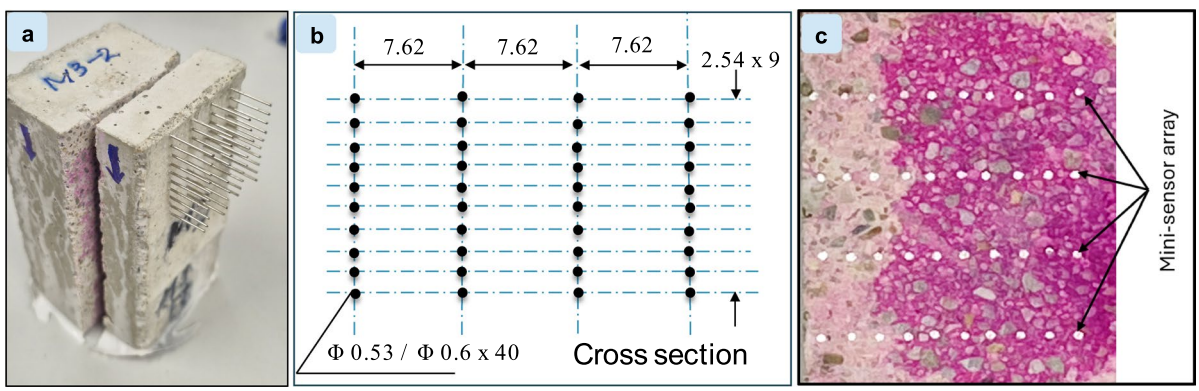

Fig. 2 Overview of the sensor configuration for carbonation monitoring. **a** Mortar sample with embedded sensors, showing unidirectional carbonation from top to bottom (arrow) and a split section for accuracy confirmation. **b** Blueprint of the sensor grid layout in cross-section. **c** Cross-sectional view of the mortar prism displaying the embedded sensor arrays

Table 1 Chemical composition of cement

Composotion [wt.%]	SiO_2	Al_2O_3	Fe_2O_3	CaO	MgO	SO_3	K_2O	Na_2O	LOI
CEM I 52.5R	19.6	4.5	3	62.2	3.5	3.5	1.01	0.27	2.5
Slag	36.63	13.56	0.49	39.11	8.52	0.27	0.57	0.42	−1.07*
Limestone	9	0.6	0.3	49.5	–	0.03	0.3	0.1	40.1

*The sulphide in slag will be oxidized during the LOI test, so this induces an increase of weight [24]

the cement was substituted with slag and an additional 16% with limestone.

The mini-sensors were embedded at one or both ends of each mortar prism during casting, with their placement depth controlled by adjusting their penetration into the plexiglass plate, as shown in Fig. 3a, b. This setup facilitates precise positioning of the sensors at the desired depths to monitor carbonation effects. To capture variations in carbonation progression at different depths within the cementitious matrix, two embedment depths of 12 mm and 20 mm from the exposed surface were considered. This approach allows evaluation of the method's sensitivity and reliability across a range of embedment depths, accounting for potential differences in carbonation profiles in varying relative humidities.

After casting, the prisms together with the mould were placed in a moist chamber for curing at the room temperature (about 23 °C). At the age of 3 days the plexiglass plate was removed, and the prisms were demoulded.

2.3 Carbonation testing

In this study a relative humidity of 54% and a concentration of 3% CO_2 by volume were implemented for accelerating the carbonation. After demoulding, the prism with the embedded mini-sensors was cut in the middle to two halves by a diamond saw with water cooling. After rinsing and surface drying all the surfaces of the half-prism expect the exposure front were coated with epoxy resin, to allow unidirectional carbonation as shown in Fig. 3c. Care should be taken to avoid the epoxy to contaminate the extruded part of the mini-sensors for later electrical connection. After coating, the half-prism was placed in the moist chamber with the uncoated surface upwards for continuous moist curing until the age of 14 days. Afterwards the prisms were placed in a climate chamber for drying at 20 ºC and a relative humidity of 54%. The desired relative humidity was obtained with application of a saturated solution of $Mg(NO_3)_2$. Already when drying start the conductivity measurements were initiated and followed the drying for 14 days after which the samples were placed in the carbonation chamber. The relative conductivity (*RC*) and its change due to carbonation (*RCC*) in specimens are defined according to Eq. (1) and (2). These equations capture the relative changes in conductivity to account for carbonation specific to each sample with inclusion of the effect of drying on electrical properties.

$$\mathrm{RC}_{x,t} = \left(\sigma_{x,t}/\sigma_{x,0}\right)/\left(\sigma_{\mathrm{xm},t}/\sigma_{\mathrm{xm},0}\right) \tag{1}$$

$$\mathrm{RCC} = \left(\mathrm{RC}_{\mathrm{CO_2}} - \mathrm{RC}_{\mathrm{Drying}}\right)/\mathrm{RC}_{\mathrm{Drying}} \tag{2}$$

where $s_{x,t}$ is the conductivity measured at depth x and exposure duration t (including drying). Subscript xm indicates the maximum depth and 0 indicates the initial time.

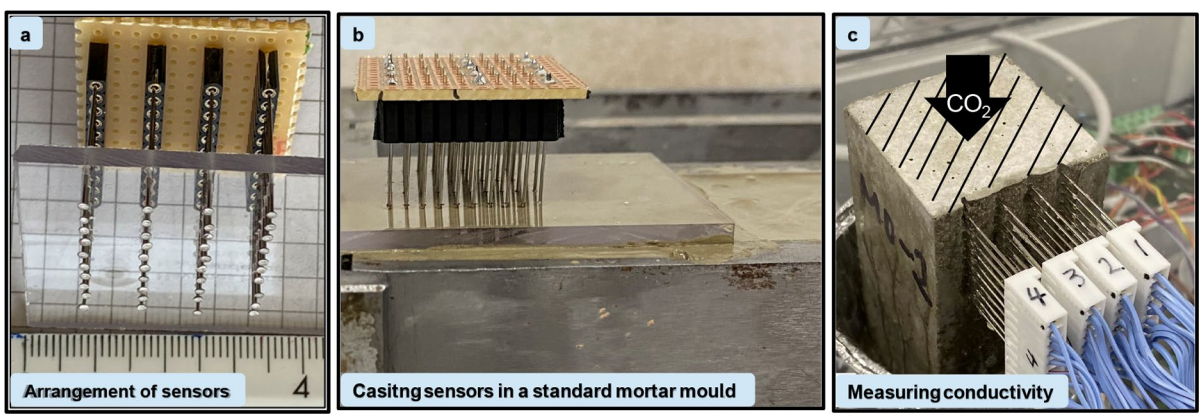

Fig. 3 Embedding mini-sensors during casting. **a** Arrangement of sensors, **b** casting sensors in a standard mortar prism and **c** allocation of sensors while measuring conductivity

2.4 Carbonation front

The carbonation front was detected using the colorimetric method to be compared with the detected values through conductivity measurements. In this method, as described in EN 13295:2004 [3], a pH indicator solution (phenolphthalein) was sprayed onto a freshly broken cementitious surface. The carbonation depth was identified as the boundary where the color change occurred, indicating the transition from a high to a low pH environment. Through conductivity measurements, carbonation front was detected, at the point at which the RCC reached -100%. To assess the correlation between the conductivity method and the colorimetric method for detecting carbonation depth, two samples were tested for each technique. The results from the two samples were averaged to emphasize the overall relationship between the methods. The coefficient of variation (COV) for each measurement point was calculated and found to fall within a range of 5–10%.

BSEM, coupled with energy-dispersive X-ray spectroscopy (EDX), was further employed to identify the carbonation front and to investigate the effect of CO_2 propagation on the elemental composition of the cementitious matrix. The boundary between carbonated and non-carbonated zones, previously identified through the colorimetric method, was marked by saw cutting for samples carbonated for 28 and 70 days, respectively. The cross-sections of these samples were polished and coated with gold before microscopy analysis. Using an FEI Quanta 200 FEG electron microscope with an accelerating voltage of 20–25 kV under high vacuum conditions, the morphology and elemental distribution across carbonated and non-carbonated zones were studied.

3 Results and discussions

3.1 Electrical properties through carbonation versus drying process

The relative conductivity of the mortar samples as a function of carbonation depth and with respect to curing regime, is presented in Fig. 4. After curing, the samples were dried for 14 days and then subjected to carbonation. The samples with natural CO_2 exposure are presented in Fig. 4a and the samples with followed exposure to 3% CO_2 are presented in Fig. 4b. Results infer that both scenarios follow a similar behaviour in agreement with previously reported results on the effect of curing on the electrical resistivity of cementitious materials [25].

Accelerated carbonation, however, induces a reduction in relative conductivity or increment in resistivity to an extent higher than drying in natural air. Given that in both curing processes drying in 54% relative humidity is actual, the difference between the two scenarios is due to the effect of accelerated carbonation on the pore system's physics and chemistry, specifically reduction in connected porosity and the conductivity of the pore solution. The reduction in porosity as a result of carbonation is well documented in literature [2], however the effect of carbonation on pore solution chemistry is two sided. Firstly, reduction of porosity could concentrate the pore solution and consequently increase its conductivity. However,

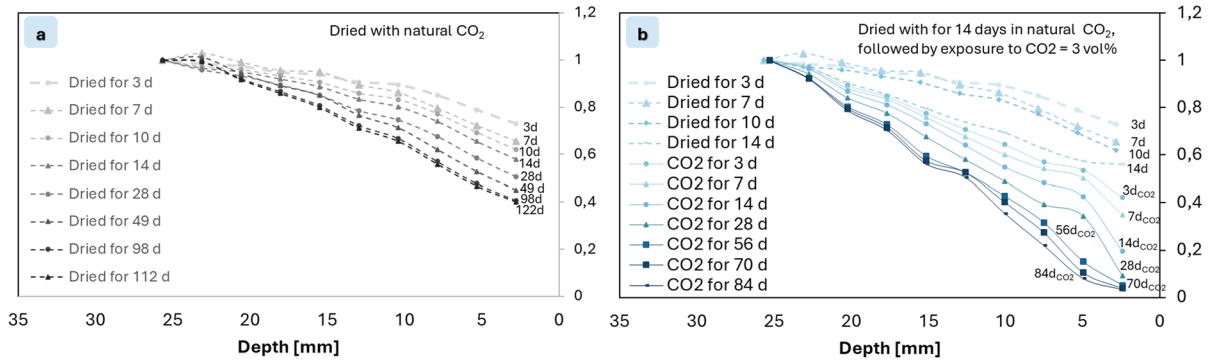

Fig. 4 Relative conductivity during natural and accelerated carbonation for sensors embedded at 12 mm depth. **a** Shows drying in natural CO_2, while **b** shows drying in natural CO_2 followed by exposure to 3 vol% CO_2

as the carbonation reactions aside from carbonates also produce free water, the pore solution can therefore be further diluted, and its conductivity is reduced. Consequently, the effect of carbonation on pore solution chemistry is a balance between changes in porosity and the progression of carbonation reactions. To separate the effect of drying from carbonation on relative conductivity, as detailed in Eq. (2), RCC parameter, the change of relative conductivity due to drying, is taken into consideration. Fig. 5 demonstrates that the long-term effect of drying on conductivity can be described by regression with power relation using only few short-term experimentally measured data. Consequently, through extrapolation, long-term evolution of relative conductivity due to drying can be predicted and utilized in Eq. (2). The results are comparable and credential for two embedment depths of mini-sensors as presented in Fig. 5. Fig. 5a, c illustrate the evolution of drying, which can be described using a power-law regression. Meanwhile, Fig. 5b, d show the results for longer drying times, which correlate well with a regression based on the first four data points and then extrapolated to longer durations.

3.2 Experimental evaluation of the monitoring system in an OPC based system

The accelerated carbonation depth (XC) and weight loss as a function of square root of time, is presented

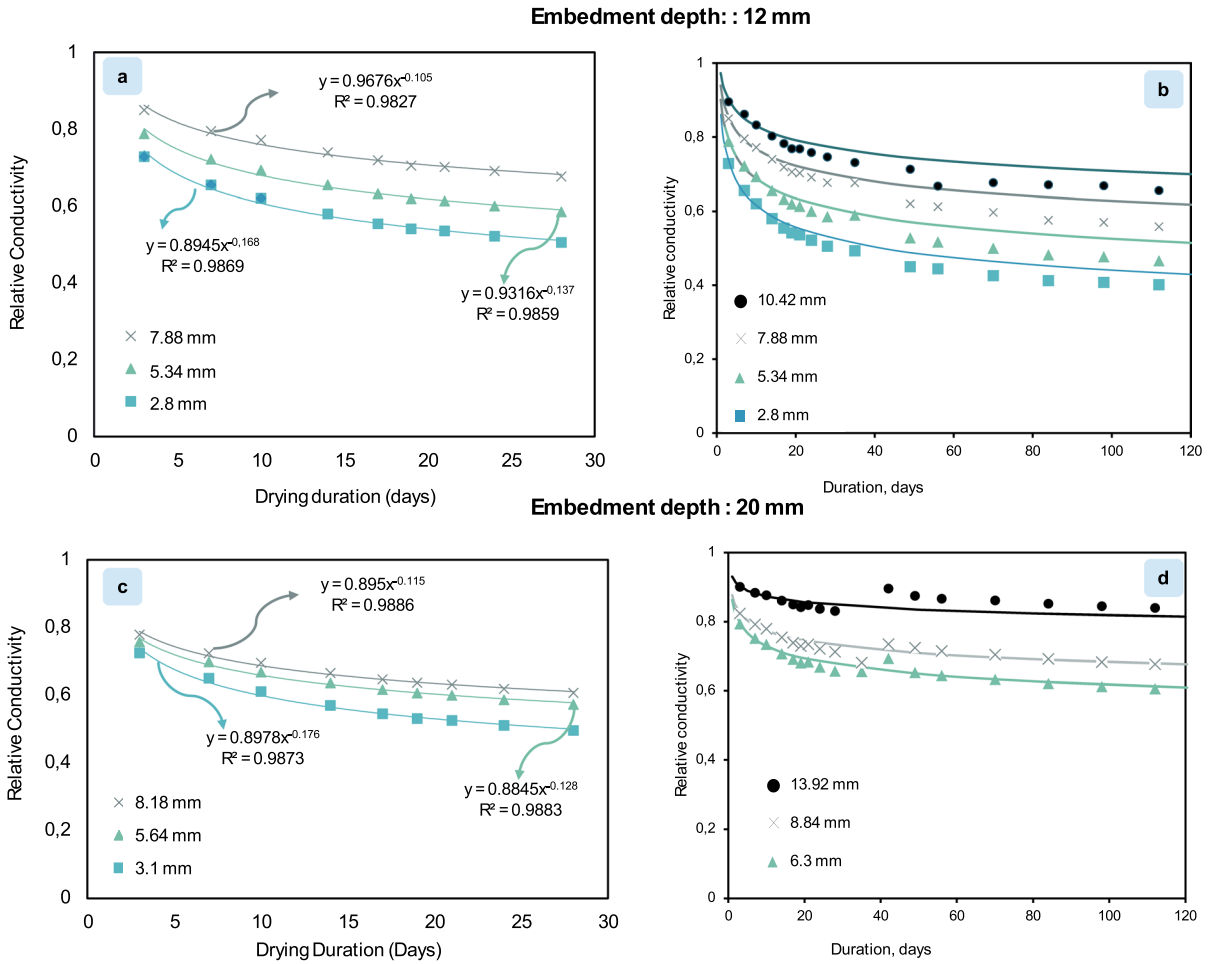

Fig. 5 Evolution of relative conductivity due to drying over time, fitted with a power-law regression for embedment depths of **a** 12 mm and **c** 20 mm. Correlation of relative conductivity at longer drying times, using a regression based on the first four data points and extrapolated for extended durations, shown for embedment depths of **b** 12 mm and **d** 20 mm

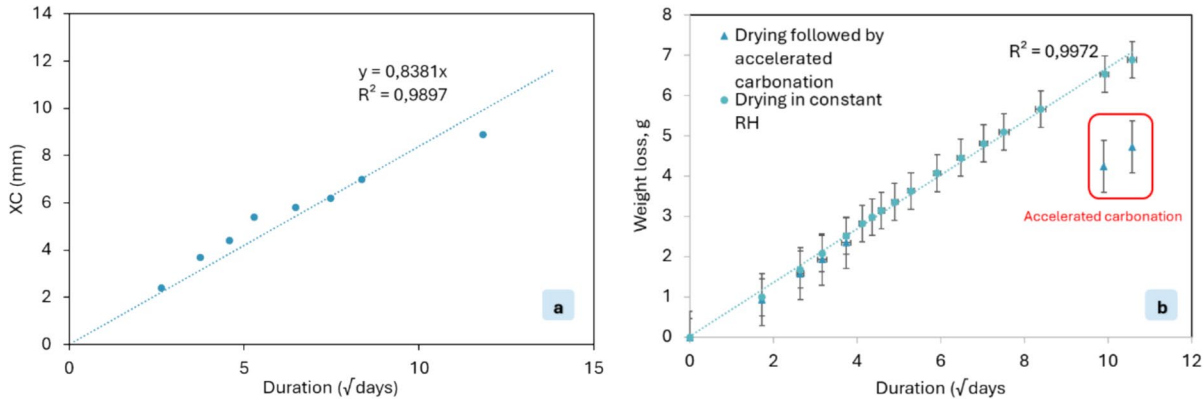

Fig. 6 **a** Accelerated carbonation depth, XC, measured using the colorimetric method, and **b** weight loss during natural and accelerated carbonation, both plotted as a function of the square root of time. In **a**, data points represent the average of two measurements. In **b**, data points represent the average of three measurements, with error bars indicating the standard deviation

in Fig. 6 (a and b respectively). In this study the accelerated carbonation maintains a linear relationship with square root of time as shown in Fig. 6a, which is a testimony to the function of the carbonation chamber developed. As presented in Fig. 6b, the relationship between weight loss and the square root of time during natural carbonation is linear. However, in accelerated carbonation the samples seem to have a lower weight loss compared to the ones exposed to natural carbonation. This behavior is firstly due to the sequestration of CO_2 into the solid phases. Secondly, although carbonation results in the production of water alongside carbonates, the generated water takes time to get dried. Both factors hence resulted in lower weight loss in samples undergoing accelerated carbonation.

Fig. 7 shows RCC values through conductivity measurements as a function of depth accounting for propagation of carbonation front. The results are presented for two tested embedment depths of sensors, i.e. 12 mm and 20 mm. From deep in the tested specimens towards CO_2 exposure surface the conductivity values follows a constant value around 0% until entering a gradual drop, a sudden peak, and a deep drop

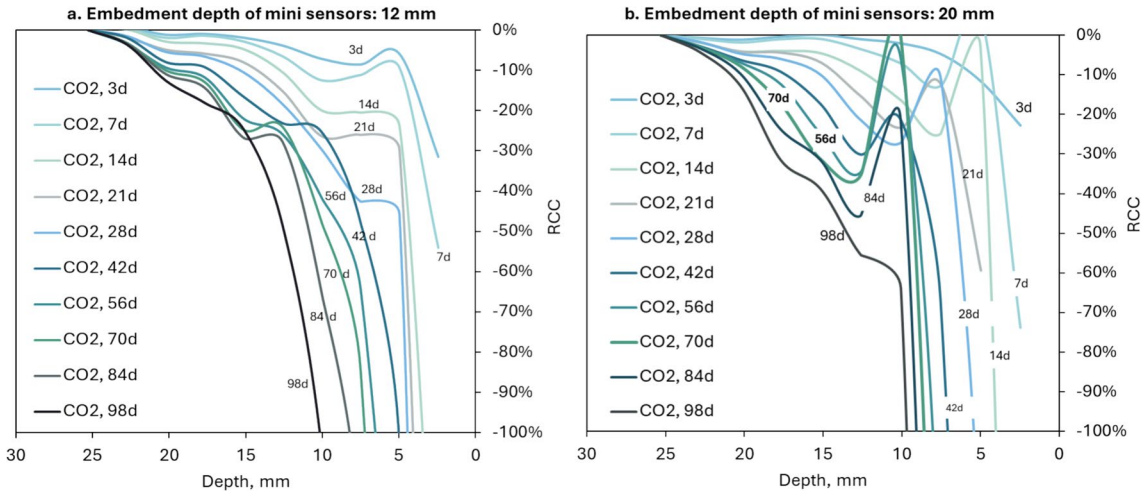

Fig. 7 Evolution of RCC in time for embedment depth of sensors at **a** 12 mm and **b** 20 mm and as a function of depth

until reaching -100%. The sudden peak followed by a sharp drop may indicate the reaction front (or partial carbonation zone), as referenced in [26]. This behaviour is likely due to the production of water during carbonation reactions. While water can dilute the pore solution and reduce its conductivity, it can also influence pore connectivity, which has a greater impact on conductivity, as noted in [27]. A chloride peak has also been reported in carbonated concrete [28–30], which could be another potential reason for the peak indicated by conductivity measurements. However, given the very low contents of chlorides in these laboratory-scale produced samples, the likelihood of the peak being entirely related to chloride zoning is very low. The difference detected in peaking behaviour between two embedment depths, can be explained by variations in relative humidity in different depth as theoretically there exist a moisture profile in depth scale of the samples.

The XC obtained by conductivity measurements as a function of time (square root of time) is presented in Fig. 8a. The XC data obtained from conductivity measurements maintain a linear relationship with the square root of time. The embedment depth of the sensors seems to have a slight effect on the value of regression parameter, being higher for the deeper embedment. In Fig. 8b, XC obtained by conductivity measurements as a function of XC from colorimetric method are presented. The results are presented with consideration of both embedment depth (12 and 20 mm). While the embedment depth of the sensors shows a slight difference in the indication of the carbonation front, there is a strong linear correlation between the carbonation depths obtained from conductivity measurements and those measured by the colorimetric method, with regression factors of 0.99 for both depths. The average difference between the two embedment depths is 1.059 mm. It is important to note that the colorimetric method can be somewhat arbitrary, as it relies on pH and the subjective judgment of the reader, as well as the accuracy of depth measurements. This minor difference may also be attributed to variations in the relative humidity profile at different depths within the sample. Shallower penetration depths typically result in lower relative humidity, which in turn leads to reduced carbonation potential. This point requires further investigation and reflects on the importance of relative humidity in designing accelerated carbonation practices in cementitious materials.

The BSEM results coupled with EDX analysis accounting for the effect of CO_2 propagation on elemental composition within the cementitious matrix are presented in Fig. 9. BSEM is shown as a powerful tool to identify the interfacial transition zone by mapping and line scanning [31]. Due to the high volume of sand in samples, the mapping results presented in Fig. 9 does not show any evident differences between the carbonated and non-carbonated zone of samples after 28 d as well as for samples after 70 d (see in Appendix). The presence of sand will strongly impact the statistical analysis of Ca, Si, and Al distribution,

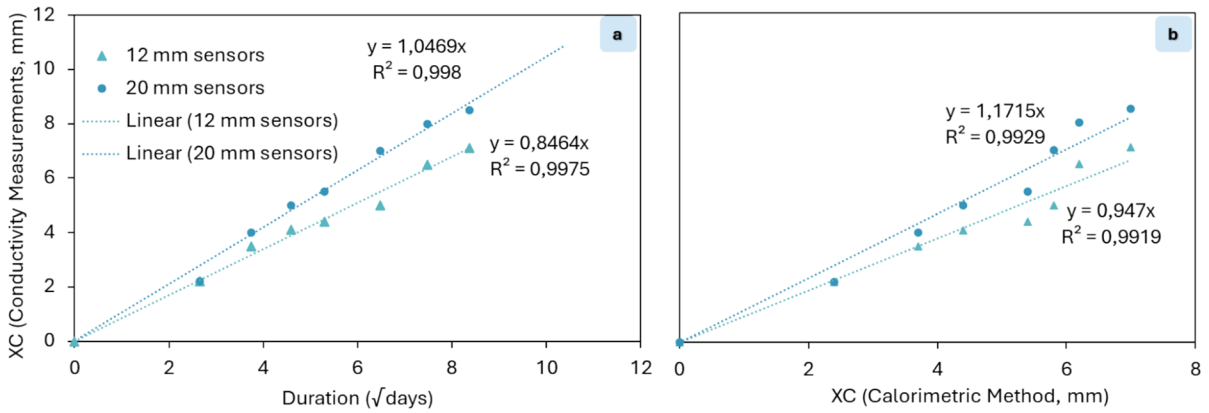

Fig. 8 **a** Accelerated carbonation depth (XC) obtained from conductivity measurements plotted against the square root of time. **b** XC values from conductivity measurements compared to those from the colorimetric method. Each data point represents the average of two measurements from separate specimens for both methods

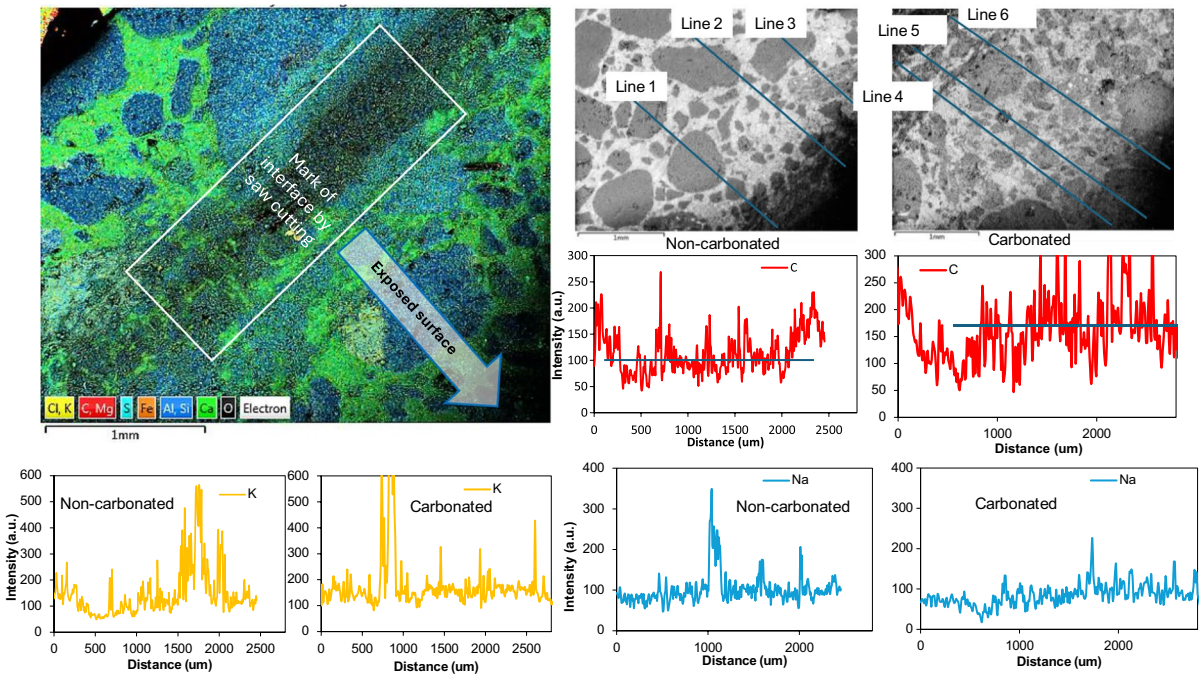

Fig. 9 Back scattering images of the polished sample after carbonation of 28 d, with mapping and line scan of elements. The elemental distribution is the average value of three scanning lines. The profile of the non-carbonated sample is based on the average values from Lines 1 to 3, while the profile of the carbonated sample is based on the average values from Lines 5 to 6

which basically represents the volume of aggregates on each line. Therefore, the analysis focuses on the carbon element (C), as it is the primary compound introduced during carbonation. The results show that the intensity of carbon in the carbonated zone is approximately 1.6 times higher than in the non-carbonated zone. Notably, the critical depth at which carbon intensity begins to decrease extends slightly beyond the boundary marked by the traditional colorimetric method for both 28 days (Fig. 9) and 70 days (Fig. 12). The carbonation depth derived from electrical conductivity shows a similar tendency, that is a bit shorter for 12 mm embedment but longer for 20 mm embedment than the colorimetric method (Fig. 8). Previous investigations found that the alkali ions will redistribute during the moisture transport and carbonation processes [32, 33] and that the concentration of alkali ions in pore solution determines the conductivity of concrete [24]. Hence, the distribution of K and Na in matrix was also analysed. Some accumulation of K or Na was identified due to the composition of sands. When focusing the analysis on the paste component of the sample, the intensity of K and Na was similar in both the carbonated and non-carbonated zones. This implies that the redistribution of alkali ions is negligible for samples subjected to carbonation, so the conductivity of mortar has not been interfered by the redistribution of alkali ions in this study.

3.3 Applicability of the method in SCM incorporated systems

The outcomes for the ternary binder system with slag and limestone are presented in Fig. 10. Fig. 10a presents the RCC values through conductivity measurements as a function of depth. The RCC value remains relatively constant at around 0%, in the deeper portions of the sample. The sudden peaking behavior before the deep drop is accounted as the reaction front, as discussed in (Sect. 3.2). To validate the method, carbonation depths were obtained using both the conductivity and colorimetric techniques. Fig. 10b illustrates

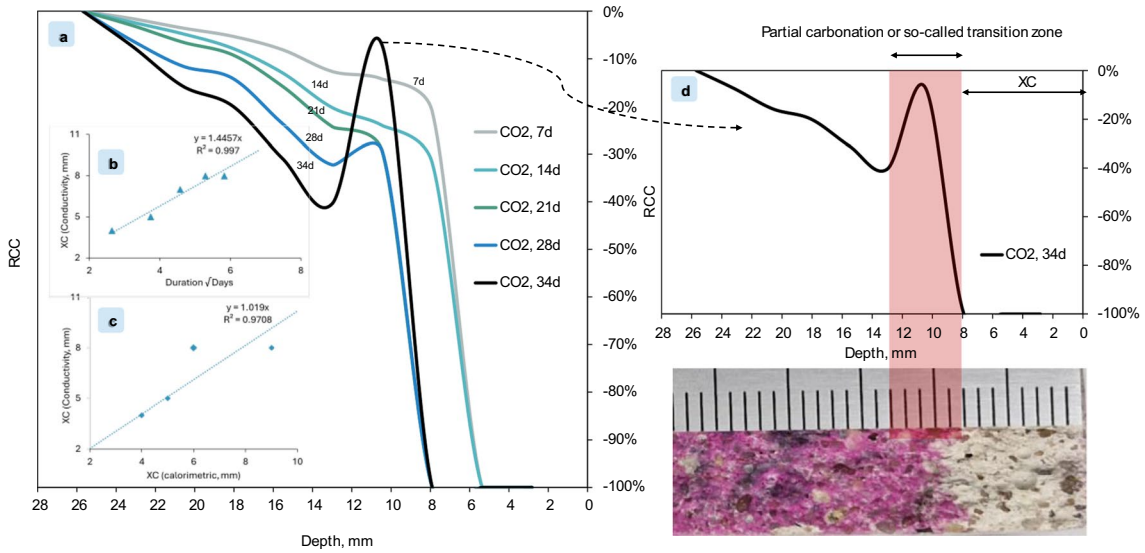

Fig. 10 **a** RCC as a function of depth for specimens containing slag and limestone. **b** XC (accelerated carbonation depth) derived from conductivity measurements plotted against the square root of time. **c** Comparison of XC values obtained by conductivity measurements and the colorimetric method, where each data point represents the average of two separate measurements (from different specimens). **d** Visualization of the carbonation front detected by conductivity measurements compared to the carbonation depth determined by the colorimetric method after 34 days

the XC values derived from conductivity measurements plotted against the square root of time, while Fig. 10c offers a comparative analysis of these values alongside those obtained from the colorimetric method. Notably, the outcomes reveal a linear relationship between the XC data from conductivity measurements and the square root of time, suggesting a consistent progression in carbonation behavior throughout the evaluated period. Also, the carbonation depths from both methods show a linear correlation with $R^2 = 0.99$, indicating a good agreement between the two methods.

However, although the carbonation depth obtained from both methods exhibit a close correlation, the colorimetric method does not capture the partial carbonation zone as illustrated in Fig. 10d. As presented in Fig. 10d, following the carbonation depth, the peak of the reaction front is observed through conductivity measurements, which can be identified as the partial carbonation zone, highlighted in a red stripe in Fig. 10d. Hence, as noted earlier as also reported in previous studies [34], the partial carbonation zone is one detail that cannot be detected through the colorimetric method.

4 Conclusions

In summary, this study introduces a non-destructive, lab-scale approach for monitoring carbonation propagation in cementitious systems through intrinsic electrical property measurements. The method's credibility is validated by comparison with colorimetric analysis, confirming its ability to accurately reflect carbonation front progression. By employing embedded mini-sensors within mortar specimens, real-time electrical property measurements enable continuous monitoring of carbonation in small samples. The inclusion of SCM-incorporated systems (slag and Limestone) further confirmed the method's applicability, demonstrating that it can reliably monitor carbonation in systems with supplementary cementitious materials.

The results demonstrate good agreement with colorimetric measurements, showing a notable decrease in conductivity at the carbonation front. This decreases, along with a preceding peak in conductivity, allows for the identification of an active carbonation reaction zone. In this zone, a distinct pattern in conductivity changes was observed: an initial increase,

followed by a subsequent decrease as the carbonation front advances. This peak behaviour at the carbonation front is likely due to water production from carbonation reactions, which can influence pore connectivity, leading to a sudden increase in conductivity. Recognizing this pattern enables users to reliably identify the carbonation front and the zone where carbonation is actively progressing, which is not possible with the colorimetric method. The carbonation front should be considered the point where RCC equals -100%, while the preceding peak indicates the zone of active carbonation. This approach presents further advantages in terms of cost-effectiveness, simplicity, and non-destructiveness compared to traditional methods, requiring fewer samples for analysis.

Backscattering microscopy analysis further identified the carbonated and non-carbonated zones based on elemental carbon distribution, confirming that alkali redistribution is negligible for affecting electrical conductivity.

The use of two embedment depths for mini-sensors also revealed the significant effect of moisture profiles within the specimen on carbonation detection, highlighting the adaptability of this method for various sample conditions. It should therefore be noted that, while this study demonstrates the method's effectiveness in a controlled lab environment, adapting it for natural conditions with variable moisture cycles and curing effects will require further research. Future studies should investigate how wet/dry cycles, complex moisture transport, and environmental factors may influence conductivity measurements, enabling the method's use in practical field applications for carbonation monitoring.

Author contributions Conceptualization: Arezou Babaahmadi, Tang Luping; Methodology: Arezou Babaahmadi, Tang Luping, Liming Huang; Formal analysis and investigation: Arezou Babaahmadi, Tang Luping, Liming Huang, Sahar Iftikhar; Writing—original draft preparation: Arezou Babaahmadi; Writing—review and editing: Arezou Babaahmadi, Luping Tang, Liming Huang, Sahar Iftikhar, Ingemar Löfgren; Funding acquisition: Arezou Babaahmadi; Resources: Arezou Babaahmadi; Supervision: Arezou Babaahmadi, Luping Tang.

Funding Open access funding provided by Chalmers University of Technology. The work is funded by the Family Thomas Foundation.

Data availability Data will be available on reasonable request.

Declarations

Conflict of interest None.

Appendix

BSEM and elemental distribution of samples after subjected to carbonation for 70 days (Figs. 11 and 12).

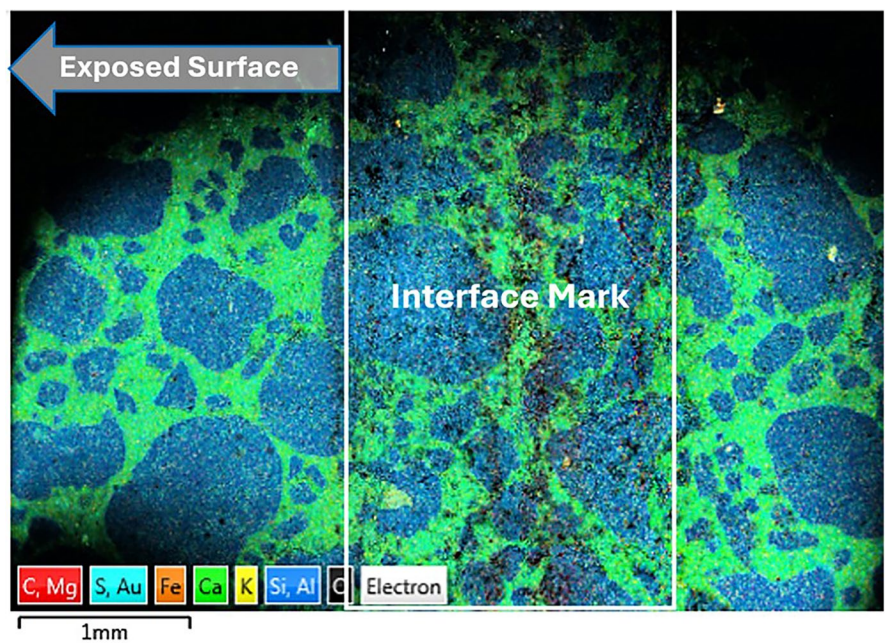

Fig. 11 BSE images of polished surface for samples after 70 d of carbonation

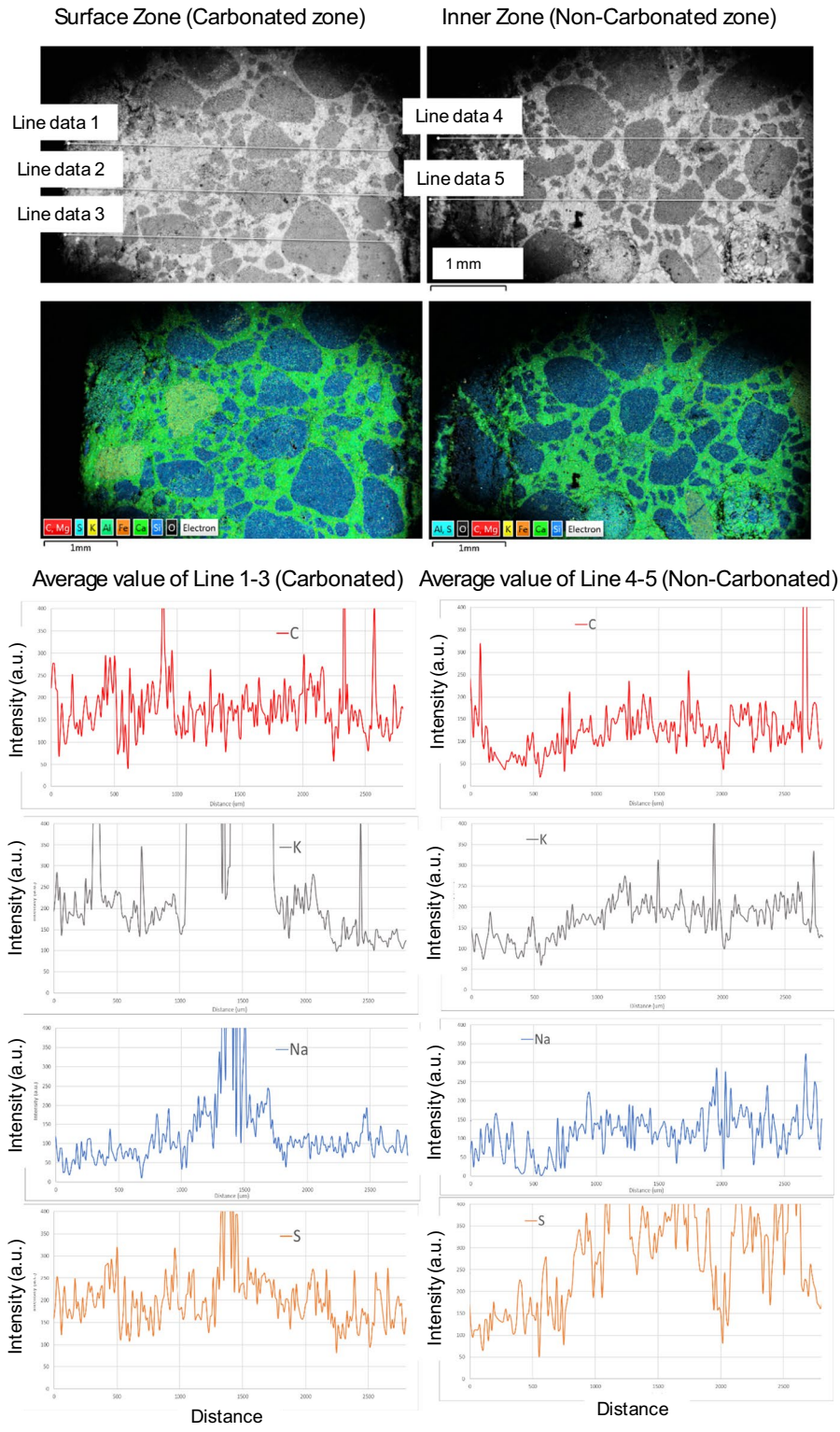

Fig. 12 BSE images of the carbonated and non-carbonated zone for samples after 70 d, with the average distribution of elements in each zone. The profile of the non-carbonated sample is based on the average values from Lines 1 to 3, while the profile of the carbonated sample is based on the average values from Lines 5 to 6

References

1. Scrivener KL, John VM, Gartner EM (2018) Eco-efficient cements: potential economically viable solutions for a low-CO2 cement-based materials industry. Cem Concr Res 114:2–26. https://doi.org/10.1016/j.cemconres.2018.03.015
2. von Greve-Dierfeld S, Lothenbach B, Vollpracht A, Wu B, Huet B, Andrade C et al (2020) Understanding the carbonation of concrete with supplementary cementitious materials: a critical review by RILEM TC 281-CCC. Mater Struct 53(6):136. https://doi.org/10.1617/s11527-020-01558-w
3. European Committee for Standardization (CEN) (2004) Products and systems for the protection and repair of concrete structures—test methods—determination of resistance to carbonation (EN 13295:2004). Belgium, Brussels, p 2004
4. Gluth GJG, Arbi K, Bernal SA, Bondar D, Castel A, Chithiraputhiran S et al (2020) RILEM TC 247-DTA round robin test: carbonation and chloride penetration testing of alkali-activated concretes. Mater Struct 53(1):21. https://doi.org/10.1617/s11527-020-1449-3
5. Telford WM, Geldart LP, Sheriff RE (1990) Applied Geophysics. Cambridge University Press, Cambridge
6. Chambers JE, Wilkinson PB, Penn S, Meldrum PI, Kuras O, Loke MH et al (2013) River terrace sand and gravel deposit reserve estimation using three-dimensional electrical resistivity tomography for bedrock surface detection. J Appl Geophys 93:25–32. https://doi.org/10.1016/j.jappgeo.2013.03.002
7. Loke MH, Chambers JE, Rucker DF, Kuras O, Wilkinson PB (2013) Recent developments in the direct-current geoelectrical imaging method. J Appl Geophys 95:135–156. https://doi.org/10.1016/j.jappgeo.2013.02.017
8. van Schoor M (2002) Detection of sinkholes using 2D electrical resistivity imaging. J Appl Geophys 50(4):393–399. https://doi.org/10.1016/S0926-9851(02)00166-0
9. McCarter WJ, Garvin S, Bouzid N (1988) Impedance measurements on cement paste. J Mater Sci Lett 7(10):1056–1057. https://doi.org/10.1007/BF00720825
10. McCarter WJ, Brousseau R (1990) The A.C. response of hardened cement paste. Cem Concr Res 20(6):891–900. https://doi.org/10.1016/0008-8846(90)90051-X
11. McCarter WJ, Chrisp TM, Starrs G, Blewett J (2003) Characterization and monitoring of cement-based systems using intrinsic electrical property measurements. Cem Concr Res 33(2):197–206. https://doi.org/10.1016/S0008-8846(02)00824-4
12. Brantervik K, Niklasson GA (1991) Circuit models for cement based materials obtained from impedance spectroscopy. Cem Concr Res 21(4):496–508. https://doi.org/10.1016/0008-8846(91)90099-4
13. Gu P, Xie P, Beaudoin JJ, Brousseau RAC (1992) impedance spectroscopy (I): a new equivalent circuit model for hydrated portland cement paste. Cem Concr Res 22(5):833–840. https://doi.org/10.1016/0008-8846(92)90107-7
14. Xie P, Gu P, Xu Z, Beaudoin JJ (1993) A rationalized a.c. impedence model for microstructural characterization of hydrating cement systems. Cem Concr Res 23(2):359–367. https://doi.org/10.1016/0008-8846(93)90101-E
15. Christensen BJ, Coverdale T, Olson RA, Ford SJ, Garboczi EJ, Jennings HM et al (1994) Impedance spectroscopy of hydrating cement-based materials: measurement, interpretation, and application. J Am Ceram Soc 77(11):2789–2804. https://doi.org/10.1111/j.1151-2916.1994.tb04507.x
16. European Committee for Standardization (CEN) (2003) Testing of hardened concrete—Part 19: determination of electrical resistivity (EN 12390–19:2023). Belgium, Brussels
17. Levita G, Marchetti A, Gallone G, Principallo A, Guerrini GL (2000) Electrical properties of fluidified Portland cement mixes in the early stage of hydration. Cem Concr Res 30(6):923–930. https://doi.org/10.1016/S0008-8846(00)00282-9
18. Heikal M, Morsy MS, Radwan MM (2005) Electrical conductivity and phase composition of calcium aluminate cement containing air-cooled and water-cooled slag at 20, 40 and 60 °C. Cem Concr Res 35(7):1438–1446. https://doi.org/10.1016/j.cemconres.2004.09.027
19. McCarter WJ, Chrisp TM, Starrs G, Basheer PAM, Blewett J (2005) Field monitoring of electrical conductivity of cover-zone concrete. Cement Concr Compos 27(7):809–817. https://doi.org/10.1016/j.cemconcomp.2005.03.008
20. Wang Y, Nanukuttan S, Bai Y, Yang K, Basheer PM (2018) Electrical resistance to monitor carbonation and chloride ingress. ACI Mater J. https://doi.org/10.14359/51716834
21. Huang L, Tang L, Löfgren I, Olsson N, Babaahmadi A, Esping O et al (2023) Non-destructive test system to monitor hydration and strength development of low CO2 concrete. Constr Build Mater 408:133774. https://doi.org/10.1016/j.conbuildmat.2023.133774
22. Elkhaldi I, Roziere E, Villain G, Loukili A (2024) Effect of accelerated carbonation on electrical resistivity and microstructure of clinker-slag-limestone cement based

concretes. Mater Struct 57(1):17. https://doi.org/10.1617/s11527-023-02290-x
23. Wilson W, Georget F, Scrivener K (2021) Unravelling chloride transport/microstructure relationships for blended-cement pastes with the mini-migration method. Cem Concr Res 140:106264. https://doi.org/10.1016/j.cemconres.2020.106264
24. Huang L, Tang L, Löfgren I, Olsson N, Yang Z (2022) Real-time monitoring the electrical properties of pastes to map the hydration induced microstructure change in cement-based materials. Cement Concr Compos 132:104639. https://doi.org/10.1016/j.cemconcomp.2022.104639
25. Chen L, Ley MT (2023) Real-time measurement of mortar properties with electrical resistivity during curing. J Mater Civ Eng 35(11):04023380. https://doi.org/10.1061/JMCEE7.MTENG-15649
26. Meier SA, Peter MA, Muntean A, Böhm M (2007) Dynamics of the internal reaction layer arising during carbonation of concrete. Chem Eng Sci 62(4):1125–1137. https://doi.org/10.1016/j.ces.2006.11.014
27. Rajabipour F, Weiss J (2007) Electrical conductivity of drying cement paste. Mater Struct 40(10):1143–1160. https://doi.org/10.1617/s11527-006-9211-z
28. Guo B, Qiao G, Han P, Li Z, Fu Q (2022) Effect of natural carbonation on chloride binding behaviours in OPC paste investigated by a thermodynamic model. J Build Eng 49:104021. https://doi.org/10.1016/j.jobe.2022.104021
29. Suryavanshi AK, Narayan SR (1996) Stability of Friedel's salt in carbonated concrete structural elements. Cem Concr Res 26(5):729–741. https://doi.org/10.1016/S0008-8846(96)85010-1
30. Backus J, McPolin D, Basheer M, Long A, Holmes N (2013) Exposure of mortars to cyclic chloride ingress and carbonation. Adv Cem Res 25(1):3–11. https://doi.org/10.1680/adcr.12.00029
31. Huang L, Yu L, Zhang H, Yang Z (2019) Composition and microstructure of 50-year lightweight aggregate concrete (LWAC) from Nanjing Yangtze River bridge (NYRB). Constr Build Mater 216:390–404. https://doi.org/10.1016/j.conbuildmat.2019.05.015
32. Dow C, Glasser FP (2003) Calcium carbonate efflorescence on Portland cement and building materials. Cem Concr Res 33(1):147–154. https://doi.org/10.1016/S0008-8846(02)00937-7
33. Yang Z, Xue N, Xu L, Yu L, Huang L, Wu K (2023) Evaluation of the efflorescence resistance of calcium sulfoaluminate cement mortar: from indoor accelerated testing to outdoor exposure. J Market Res 22:2447–2461. https://doi.org/10.1016/j.jmrt.2022.12.061
34. Bernal SA, Dhandapani Y, Elakneswaran Y, Gluth GJG, Gruyaert E, Juenger MCG et al (2024) Report of RILEM TC 281-CCC: a critical review of the standardised testing methods to determine carbonation resistance of concrete. Mater Struct 57(8):173. https://doi.org/10.1617/s11527-024-02424-9